Inorganic Chemistry
Article

Inorg. Chem. **2009**, *48*, 7691–7697 **7691**
DOI: 10.1021/ic9004533

Structural, Luminescent, and Magnetic Properties of Three Novel Three-Dimensional Metal-Organic Frameworks Based on Hexadentate *N,N′*-bis(4-picolinoyl)hydrazine

Zhen-Lan Fang, Rong-Min Yu, Jian-Gang He, Qi-Sheng Zhang, Zhen-Guo Zhao, and Can-Zhong Lu*

The State Key Laboratory of Structural Chemistry, Fujian Institute of Research on the Structure of Matter, The Chinese Academy of Sciences, Fuzhou, Fujian 350002, P.R. China

Received March 7, 2009

Three novel microporous three-dimensional (3-D) metal-organic framework materials $[ML]_n$ [M = Ni, Co, Cd; L = *N,N′*-bis(4-picolinoyl)hydrazine] were obtained from hydrothermal reactions. The organic ligand L was formed through the in situ ring-opening hydrolysis reaction of 2,5-bis(4-pyridyl)-1,3,4-oxadiazole with the assistance of metal ions. Single-crystal X-ray diffraction studies reveal that complexes **1**−**3** adopt 6-connected 3-D networks of distorted α-Po topology, which are built from non-interpenetrated (4,4) grids cross-linked by zigzag chains. These isomorphic complexes are all of high thermal stability, but some other physical properties are quite different because of their different metal centers. Antiferromagnetic exchange was observed between Ni(II) centers of complex **1**, while ferromagnetic for Co(II) centers of complex **2**. Complex **3** exhibits strong fluorescence emission.

Introduction

Microporous metal-organic frameworks (MOFs) as a new class of Zeolite-type materials have attracted much attention in recent years, owing to their intriguing topologies and various potential applications in gas storage, catalysis, ion exchange, luminescence, and magnetism.[1−11] To obtain such MOF materials, many researchers commonly use rigid and extended organic ligands in backbone such as carboxylates,[12−14] nitrogen containing heterocyclic compounds (e.g., pyridines,[15] midazoles,[16] triazoles,[17] and tetrazoles[11,18]), and organic compounds with both multicarboxylate and heterocyclic groups.[19] Recently, as one kind of these rigid and extended ligands, the coordination chemistry of oxadiazole-containing dipyridyl, such as the series of 2,5-bis-(2-pyridyl)-1,3,4-oxadiazole, 2,5-bis(3-pyridyl)-1,3,4-oxadiazole, and 2,5-bis(4-pyridyl)-1,3,4-oxadiazole, have been investigated extensively for their unique angular geometry and versatile bonding modes. A variety of discrete and infinite coordination architectures based on such kind of bridging ligands have been achieved;[20,21] however, the complexes as zeolite-type microporous materials are scarce. To further develop the understanding of the construction of MOFs based on such ligands, we preformed the reactions of 2,5-bis(4-pyridyl)-1,3,4-oxadiazole with $NiCl_2 \cdot 6H_2O$, $CoCl_2 \cdot 6H_2O$, and $3CdSO_4 \cdot 8H_2O$, respectively, under hydrothermal conditions. Surprisingly, metal-assisted hydrolysis of

*To whom correspondence should be addressed. E-mail: czlu@fjirsm.ac.cn. Fax: +86-591-83714946. Phone: +86-591-83705794.

(1) Eddaoudi, M.; Kim, J.; Rosi, N.; Vodak, D.; Wachter, J.; O'Keeffe, M.; Yaghi, O. M. *Science* **2002**, *295*, 469.
(2) Kitaura, R.; Seki, K.; Akiyama, G.; Kitagawa, S. *Angew. Chem., Int. Ed.* **2003**, *42*, 428.
(3) Moulton, B.; Zaworotko, M. J. *Chem. Rev.* **2001**, *101*, 1629.
(4) Gardner, G. B.; Venkataraman, D.; Moore, J. S.; Lee, S. *Nature* **1995**, *374*, 792.
(5) Chui, S. S. Y.; Lo, S. M. F.; Charmant, J. P. H.; Orpen, A. G.; Williams, I. D. *Science* **1999**, *283*, 1148.
(6) Seo, J. S.; Whang, D.; Lee, H.; Jun, S. I.; Oh, J.; Jeon, Y. J.; Kim, K. *Nature* **2000**, *404*, 982.
(7) Miller, J. S.; Epstein, A. J. *Angew. Chem., Int. Ed.* **1994**, *33*, 385.
(8) Choudhury, A.; Neeraj, S.; Natarajan, S.; Rao, C. N. R. *Angew. Chem., Int. Ed.* **2000**, *39*, 3091.
(9) Millange, F.; Serre, C.; Ferey, G. *Chem. Commun.* **2002**, 822.
(10) Ayyappan, P.; Evans, O. R.; Lin, W. B. *Inorg. Chem.* **2001**, *40*, 4627.
(11) Li, J. R.; Tao, Y.; Yu, Q.; Bu, X. H.; Sakamoto, H.; Kitagawa, S. *Chem.—Eur. J.* **2008**, *14*, 2771.
(12) Eddaoudi, M.; Li, H. L.; Yaghi, O. M. *J. Am. Chem. Soc.* **2000**, *122*, 1391.
(13) Dai, J. C.; Wu, X. T.; Fu, Z. Y.; Hu, S. M.; Du, W. X.; Cui, C. P.; Wu, L. M.; Zhang, H. H.; Sun, R. Q. *Chem. Commun.* **2002**, 12.
(14) Galan-Mascaros, J. R.; Clemente-Juan, J. M.; Dunbar, K. R. *J. Chem. Soc., Dalton Trans.* **2002**, 2710.
(15) Ghosh, S. K.; Ribas, J.; Bharadwaj, P. K. *Cryst. Growth Des.* **2005**, *5*, 623.
(16) Qi, Y.; Luo, F.; Che, Y. X.; Zhen, J. M. *Cryst. Growth Des.* **2008**, *8*, 606.
(17) Wang, Y.; Cheng, P.; Song, Y.; Liao, D. Z.; Yanl, S. P. *Chem.—Eur. J.* **2007**, *13*, 8131.
(18) Collins, C. S.; Sun, D. F.; Liu, W.; Zuo, J. L.; Zhou, H. C. *J. Mol. Struct.* **2008**, *890*, 163.
(19) Cao, X. Y.; Li, Z. J.; Zhang, J.; Qin, Y. Y.; Cheng, J. K.; Yao, Y. G. *CrystEngComm* **2008**, *10*, 1345.
(20) Bu, X. H.; Liu, H.; Du, M.; Zhang, L.; Guo, Y. M.; Shionoya, M.; Ribas, J. *Inorg. Chem.* **2002**, *41*, 1855.
(21) Du, M.; Bu, X. H.; Huang, Z.; Chen, S. T.; Guo, Y. M.; Diaz, C.; Ribas, J. *Inorg. Chem.* **2003**, *42*, 552.

Published on Web 07/10/2009

2,5-bis(4-pyridyl)-1,3,4-oxadiazole to form *N*,*N*′-bis(4-picolinoyl)hydrazine (L) was observed. Maybe because of the flexibility of N−N bond, L presents multiple potential donor sites with many possible coordination modes. Consequently, L was further assembled with metal salts to afford a series of new three-dimensional (3-D) non-interpentrating MOFs **1**−**3** that are isomorphic. To the best of our knowledge, similar investigation on the coordination chemistry of L has seldom been explored, and the complexes **1**−**3** are the first examples of MOFs with L. One Zn(II) polymeric complex of L has been reported;[22] however, it was obtained through the condensation reaction of isoniazid with the catalysis of zinc salts having non-coordinating anions while not the hydrolysis of L. Herein, the syntheses, structures, magnetic properties, photoluminescence, and thermal stability of complexes **1**−**3** were investigated in detail.

Experimental Section

Materials and General Methods. The bridging ligand 2,5-bis(4-pyridyl)-1,3,4-oxadiazole was synthesized according to a reported literature procedure.[23] Other chemicals were obtained from commercial sources and used without further purification. The IR spectra (KBr pellets) were recorded on a Magna 750 FT-IR spectrophotometer in the range 400−4000 cm^{-1}. C, H, and N elemental analyses were determined on an EA1110 CHNS-0 CE element analyzer. Powder X-ray diffraction data were recorded on a PANaytical X'pert pro X-ray diffractometer with graphite-monochromatized Cu Ka radiation (λ = 1.542 Å). Thermal stability studies were carried out on a NETSCHZ STA 449C thermoanalyzer under N_2 (30−1200 °C range) at a heating rate of 10 K/min. Fluorescence spectra were measured on an Edinburgh Analytical instrument FLS920. The polycrystalline magnetic susceptibility data were collected on a Quantum Design PPMS model 6000 magnetometer in the temperature range from 2 to 300 K. Electron paramagnetic resonance (EPR) measurements were performed on a Bruker EMX EPR spectrometer at X-band frequency (9.46 GHz). Typically, a fixed amount of sample after pretreatment under different conditions was transferred into a quartz tube instantly, and the quartz tube was set in a quartz Dewar vessel in the EPR cavity. The temperature was set at 77 K throughout the experiment.

Synthesis of $[NiL]_n$ (1). A mixture containing $NiCl_2 \cdot 6H_2O$ (100.0 mg, 0.42 mmol), 2,5-bis(4-pyridyl)-1,3,4-oxadiazole (30.0 mg, 0.13 mmol), anhydrous ethanol (2 mL), aqueous ammonia (25%, 2 mL), and deionized water (8 mL) was placed in a Parr Teflon-lined stainless steel vessel (20 mL) under autogenous pressure, and stirred at room temperature for 5 h, which was heated at 180 °C for 24 h, followed by slow cooling to room temperature at a rate of 6 °C h^{-1}. Green block crystals of the product were collected, washed with H_2O, and air-dried. The final product yield was 52.5% based on 2,5-bis(4-pyridyl)-1,3,4-oxadiazole. Anal. Calcd(%) for $C_{12}H_{10}N_4O_2Ni$: C, 48.16; H, 2.68; N, 18.72. Found: C, 47.86; H, 2.52; N, 18.36. FT-IR (solid KBr pellet, ν/cm^{-1}): 3083(w), 1958(w), 1616(m), 1567(s), 1531(s), 1494(s), 1421(s), 1384(w), 1323(w), 1213(w), 1164(w), 1090(w), 1066(w), 1005(m), 883(w), 846(s), 760(m), 724(m), 699(s), 663(w), 614(s), 455(s).

Synthesis of $[CoL]_n$ (2). A mixture containing $CoCl_2 \cdot 6H_2O$ (300.0 mg, 1.26 mmol), 2,5-bis(4-pyridyl)-1,3,4-oxadiazole (80.0 mg, 0.36 mmol), anhydrous ethanol (2 mL), aqueous ammonia (25%, 1 or 2 mL), and deionized water (8 mL) was placed in a Parr Teflon-lined stainless steel vessel (20 mL) under autogenous pressure, and stirred at room temperature for 5 h, which was then heated at 180 °C for 24 h, followed by slow cooling to room temperature at a rate of 8 °C h^{-1}. After being washed with H_2O and air-dried, the red needle crystals of the product were obtained with final yield 41.5% based on 2,5-bis(4-pyridyl)-1,3,4-oxadiazole. Anal. Calcd(%) for $C_{12}H_{10}N_4O_2Co$: C, 48.06; H, 2.78; N, 18.77. Found: C, 47.92; H, 2.82; N, 18.56. FT-IR (solid KBr pellet, ν/cm^{-1}): 3074(w), 1962(w), 1619(s), 1571(s), 1534(s), 1485(s), 1424(s), 1375(s), 1325(w), 1214(m), 1156(m), 1081(w), 1057(m), 1008(m), 996(m), 874(w), 837(s), 751(m), 727(s), 704(s), 605(w).

Synthesis of $[CdL]_n$ (3). A mixture containing $3CdSO_4 \cdot 8H_2O$ (200.0 mg, 0.26 mmol), 2,5-bis(4-pyridyl)-1,3,4-oxadiazole (50.0 mg, 0.22 mmol), anhydrous ethanol (1.8 mL), aqueous ammonia (25%, 1.1 mL), and deionized water (8 mL) was placed in a Parr Teflon-lined stainless steel vessel (20 mL) under autogenous pressure, and stirred at room temperature for 5 h, which was heated at 180 °C for 24 h, followed by slow cooling to room temperature at a rate of 8 °C h^{-1}. Yellow needle or block crystals of the product were collected after being washed with H_2O and air-dried with final yield 36% based on 2,5-bis(4-pyridyl)-1,3,4-oxadiazole. Anal. Calcd(%) for $C_{12}H_{10}N_4O_2Cd$: C, 40.91; H, 2.28; N, 15.91. Found: C, 40.52; H, 2.32; N, 15.56. FT-IR (solid KBr pellet, ν/cm^{-1}), 3063(w), 2036(w), 1634(w), 1609(s), 1573(s), 1511(s), 1480(s), 1413(w), 1389(s), 1218(m), 1145(w), 1120(w), 1083(w), 1059(m), 1010(m), 876(w), 863(w), 753(m), 717(m), 692(s), 594(m).

X-ray Crystallography. The single crystals of the complexes in the present work were mounted on a glass fiber for the X-ray diffraction analysis. Data sets were collected on a Rigaku AFC7R equipped with a graphite-monochromated Mo KR radiation (λ = 0.71073 Å) from a rotating anode generator at 293 K. Intensities were corrected for LP factors and empirical absorption using the ψ scan technique. The structure was solved by direct methods and refined on F^2 with full-matrix least-squares techniques using the Siemens SHELXTL version 5 package of crystallographic software.[24] All non-hydrogen atoms were refined anistropically. The positions of the hydrogen atoms attached to carbon atoms were fixed at their ideal positions. Crystal data, as well as details of data collection and refinement, for complexes **1**−**3** are summarized in Table 1. The selected interatomic distances and bond angles are given in Table 2.

Computational Descriptions. The crystallographic data of complex **3** determined by X-ray was used to calculate its electronic band structure. The density functional theory (DFT) calculations[25−28] were performed on complex **3** by using the CASTEP code.[29] The total energy was calculated within the framework of the Perdew−Burke−Ernzerhof generalized gradient approximation.[30] The interactions between the ionic cores and the electrons were described by the norm-conserving pseudopotentials.[31] We chose an energy cutoff of the plane-wave of 550 eV and a 4 × 2 × 2 Monkhorst-Pack *k*-point grid for complex **3**.

(22) Koppenhofer, A.; Hartmann, U.; Vahrenkamp, H. *Chem. Ber.* **1995**, *128*, 779.
(23) Bentiss, F.; Lagrenee, M. *J. Heterocycl. Chem.* **1999**, *36*, 1029.
(24) *SHELXTLTM*, version 5, Reference Manual; Science Energy & Automation Inc.: Madison, WI, 1994.
(25) Lee, C.; Yang, W.; Parr, R. G. *Phys. Rev. B* **1988**, *37*, 785.
(26) Wiberg, K. B.; Stratmann, R. E.; Frisch, M. J. *Chem. Phys. Lett.* **1998**, *297*, 60.
(27) Wang, C. C.; Yang, C. H.; Tseng, S. M.; Lin, S. Y.; Wu, T. Y.; Fuh, M. R.; Lee, G. H.; Wong, K. T.; Chen, R. T.; Cheng, Y. M.; Chou, P. T. *Inorg. Chem.* **2004**, *43*, 4781.
(28) Bauernschmitt, R.; Ahlrichs, R.; Hennrich, F. H.; Kappes, M. M. *J. Am. Chem. Soc.* **1998**, *120*, 5052.
(29) Segall, M. D.; Lindan, P. J. D.; Probert, M. J.; Pickard, C. J.; Hasnip, P. J.; Clark, S. J.; Payne, M. C. *J. Phys.: Condens. Matter* **2002**, *14*, 2717.
(30) Perdew, J. P.; Burke, K.; Ernzerhof, M. *Phys. Rev. Lett.* **1996**, *77*, 3865.
(31) Lin, J. S.; Qteish, A.; Payne, M. C.; Heine, V. *Phys. Rev. B* **1993**, *47*, 4174.

Table 1. Crystal Data and Structure Refinement Results for Complexes **1**−**3**

	1	**2**	**3**
empirical formula	$C_{12}H_8NiN_4O_2$	$C_{12}H_8CoN_4O_2$	$C_{12}H_8CdN_4O_2$
formula weight	298.74	298.96	352.43
cryst syst	monoclinic	monoclinic	monoclinic
space group	$P2_1/c$	$P2_1/c$	$P2_1/c$
Z	2	2	2
a (Å)	4.829(2)	4.965(4)	5.290(2)
b (Å)	10.719(6)	10.781(9)	10.744(5)
c (Å)	10.981(5)	10.927(10)	10.772(5)
α (deg)	90	90	90
β (deg)	94.222(11)	93.461(19)	90.285(8)
γ (deg)	90	90	90
V (Å^3)	573.1(5)	583.8(9)	612.2(5)
ρ_{calcd} (g/cm^3)	1.732	1.702	1.913
μ (mm^{-1})	1.695	1.472	1.786
GOF	1.053	1.031	1.072
R_1 ($I > 2\sigma(I)$)[a]	0.0294	0.0298	0.0277
wR_2 (all data)[b]	0.1074	0.1077	0.1086

[a] $R_1 = \sum||F_o| - |F_c||/\sum|F_o|$. [b] $wR_2 = [\sum w(F_o^2 - F_c^2)^2/\sum w(F_o^2)^2]^{1/2}$.

Results and Discussion

Hydrolysis Mechanism. On the basis of the literature,[20] the possible hydrolysis mechanism promoted by the metal ion in two ways should be addressed: (1) the metal ion as a Lewis acid catalyzes hydrolysis reactions in neutral or basic solution; (2) the metal ion coordinates to nitrogen atom of oxadiazole, which induces that the carbon center is activated and very susceptible to nucleophilic attack by H_2O in the solvent medium. The possible hydrolysis mechanism for our reactions are shown in Scheme 1. One should be aware that a few of the possible mechanisms have been mentioned for the hydrolysis reaction facilitated by Ni, Co, and Cd while most by Cu. In addition, this is the first report on the in situ hydrolysis of 2,5-bis(4-pyridyl)-1,3,4-oxadiazole to form L with the assistance of metal ions in the preparation of hydrazine complexes.

Structure Description. Single crystal X-ray diffraction studies of complexes **1**−**3** revealed that these complexes are isomorphic. Herein, we discuss the structure of complex **1** in detail and only mention pertinent points of complexes **2** and **3**. The coordination environment of complex **1** is shown in Figure 1a. The complex **1** crystallizes in the monoclinic space group $P2_1/c$ with two Ni atoms and two L ligands in each unit cell. The metal centers are six-coordinated by two carbonyl oxygen atoms, two nitrogen atoms of hydrazine from two L ligands in the equatorial positions, and two nitrogen atoms of the pyridyl groups from another two L ligands in the axial positions, forming a slightly distorted octahedral geometry [Ni−N 2.215(2)−2.478(4) Å and Ni−O 2.019(17)−2.273(3) Å]. Meanwhile, each L ligand serves as a hexadentate ligand. It coordinates to two Ni atoms as a bis-bidentate ligand, and links two other Ni atoms just like a bipyridyl ligand. In complexes **1**−**3**, the distances between adjacent N atoms are longer than 1.4 Å illuminating a basically single bond for them, while the distances between C and O are about 1.276(3) Å (**1**), 1.286(3) Å (2), 1.275(6) Å (3), respectively, implying that they belong to a double bond. All the C−N bond lengths in these complexes have a value of ∼1.32 (9) Å, which is longer than a typical carbon−nitrogen double bond N=C [1.262(5) Å] and rather shorter than a typical carbon−nitrogen single bond N−C [1.41(5) Å]. Therefore, the electron delocalization exists in the O−C−N moiety, and L can be properly understood as a substituted hydrazine group rather than a diazene derivative, which was further testified by the IR spectrum of these complexes (Supporting Information, Figure S1). In the structure, the −(CO)NN(CO)− moiety of the L ligands is

Table 2. Selected Bond Lengths (Å) and Angles (deg) for Complexes **1**−**3**[a]

1[b]

Ni(1)−O(1)#1	2.019(17)	N(2)#3−Ni(1)−N(2)#4	180.00
Ni(1)−O(1)#2	2.019(17)	O(1)#1−Ni(1)−N(1)	89.16(8)
Ni(1)−N(2)#3	2.083(2)	O(1)#2−Ni(1)−N(1)	90.84(8)
Ni(1)−N(2)#4	2.083(2)	N(2)#3−Ni(1)−N(1)	83.05(8)
Ni(1)−N(1)	2.215(2)	N(2)#4−Ni(1)−N(1)	96.95(8)
Ni(1)−N(1)#5	2.215(2)	O(1)#1−Ni(1)−N(1)#5	90.84(8)
O(1)#1−Ni(1)−O(1)#2	180.00(10)	O(1)#2−Ni(1)−N(1)#5	89.16(8)
O(1)#1−Ni(1)−N(2)#3	101.70(7)	N(2)#3−Ni(1)−N(1)#5	96.95(8)
O(1)#2−Ni(1)−N(2)#3	78.30(7)	N(2)#4−Ni(1)−N(1)#5	83.05(8)
O(1)#1−Ni(1)−N(2)#4	78.30(7)	N(1)−Ni(1)−N(1)#5	180.00(9)
O(1)#2−Ni(1)−N(2)#4	101.70(7)		

2[c]

Co(1)−O(1)#1	2.042(2)	N(2)#3−Co(1)−N(2)#4	180.00
Co(1)−O(1)#2	2.042(2)	O(1)#1−Co(1)−N(1)	90.95(10)
Co(1)−N(2)#3	2.138(3)	O(1)#2−Co(1)−N(1)	89.05(10)
Co(1)−N(2)#4	2.138(3)	N(2)#3−Co(1)−N(1)	97.96(9)
Co(1)−N(1)	2.277(3)	N(2)#4−Co(1)−N(1)	82.04(9)
Co(1)−N(1)#5	2.277(3)	O(1)#1−Co(1)−N(1)#5	89.05(10)
O(1)#1−Co(1)−O(1)#2	180.00(10)	O(1)#2−Co(1)−N(1)#5	90.95(10)
O(1)#1−Co(1)−N(2)#3	103.24(9)	N(2)#3−Co(1)−N(1)#5	82.04(9)
O(1)#2−Co(1)−N(2)#3	76.76(9)	N(2)#4−Co(1)−N(1)#5	97.96(9)
O(1)#1−Co(1)−N(2)#4	76.76(9)	N(1)−Co(1)−N(1)#5	180.00(1)
O(1)#2−Co(1)−N(2)#4	103.24(9)		

3[d]

Cd(1)−O(1)#1	2.273(3)	N(2)#1−Cd(1)−N(2)	180.00(2)
Cd(1)−O(1)	2.273(3)	O(1)#1−Cd(1)−N(1)#2	91.28(15)
Cd(1)−N(2)#1	2.299(4)	O(1)−Cd(1)−N(1)#2	88.72(15)
Cd(1)−N(2)	2.299(4)	N(2)#1−Cd(1)−N(1)#2	99.53(15)
Cd(1)−N(1)#2	2.478(4)	N(2)−Cd(1)−N(1)#2	80.47(15)
Cd(1)−N(1)#3	2.478(4)	O(1)#1−Cd(1)−N(1)#3	88.72(15)
O(1)#1−Cd(1)−O(1)	180.00(18)	O(1)−Cd(1)−N(1)#3	91.28(15)
O(1)#1−Cd(1)−N(2)#1	108.69(13)	N(2)#1−Cd(1)−N(1)#3	80.47(15)
O(1)−Cd(1)−N(2)#1	71.31(13)	N(2)−Cd(1)−N(1)#3	99.53(15)
O(1)#1−Cd(1)−N(2)	71.31(13)	N(1)#2−Cd(1)−N(1)#3	180.00(18)
O(1)−Cd(1)−N(2)	108.69(13)		

[a] Symmetry transformations used to generate equivalent atoms are listed below. [b] **1**: (#1) $x-1, -y+1/2, z-1/2$; (#2) $-x+1, y+1/2, -z+1/2$; (#3) $x, -y+1/2, z-1/2$; (#4) $-x, y+1/2, -z+1/2$; (#5) $-x, -y+1, -z$. [c] **2**: (#1) $-x+2, y-1/2, -z+1/2$; (#2) $x+1, -y+3/2, z+1/2$; (#3) $-x+3, y-1/2, -z+1/2$; (#4) $x, -y+3/2, z+1/2$; (# 5) $-x+3, -y+1, -z+1$. [d] **3**: (#1) $-x+1, -y+1, -z$; (#2) $x-1, -y+1/2, z-1/2$; (#3) $-x+2, y+1/2, -z+1/2$.

Scheme 1. Possible Mechanism for the Hydrolysis and Complexes Formation

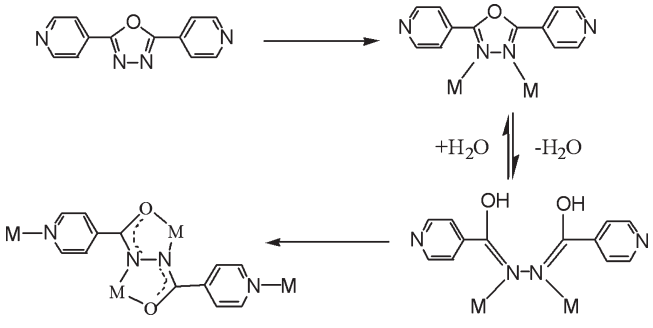

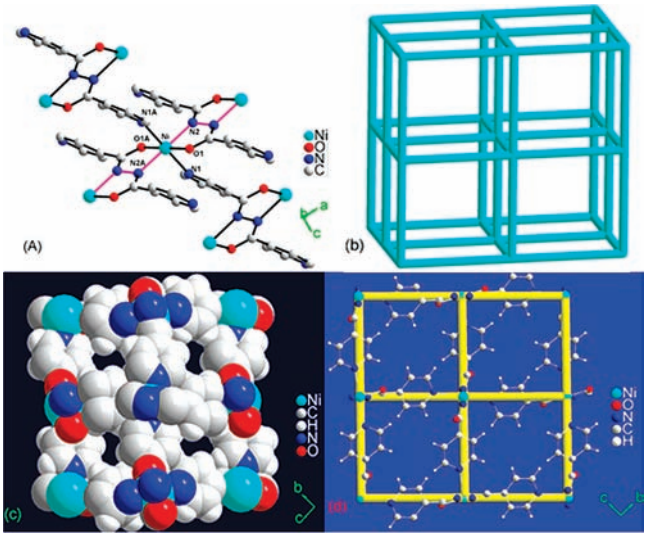

Figure 1. (a) Perspective view of coordination environments of complexes **1**−**3** show a 1-D [M−N2-N2−M]n zigzag chain; (b) The topological representation; (c) 1-D channels of 4.84 × 3.27 Å viewed along *a* axis; (d) 2-D (4,4) net in the *bc* plane. Color scheme in (a), (c), and (d): Ni, cyan; O, red; N, blue; C, white; hydrogen atoms are omitted for clarity in (a).

essentially planar (mean deviation = 0.004 Å) with the metal atom displaced from the plane by 0.057 Å, in favor of forming a new π-electron conjugated system. The pyridyl rings are twisted by 120° from the plane of the −(CO)NN(CO)− moiety. The combination of the metal centers and the ligands results in the formation of infinite 1D $[M-N-N-M]_n$ zigzag chains along the *a*-axis. The M−M distances in the one-dimensional (1-D) chains are 4.869(2), 4.965(4), and 5.290(2) Å for Ni−Ni (**1**), Co−Co (**2**), and Cd−Cd (**3**), respectively. The shortest M−M distances between 1-D chains are 7.682(3), 7.675(5), and 7.607(3) Å for Ni−Ni (**1**), Co−Co (**2**), and Cd−Cd (**3**), respectively. Complexes **1**−**3** adopt 6-connected 3-D network structures of α-Po topology that are built from the mononuclear metal center. Each mononuclear metal center acting as a node is connected to six others through four bridging L ligands to generate an extended neutral 3-D nanoporous network (Figure 1b). Accordingly, the rhombus 1-D channels of about 4.84 × 3.27 $Å^2$ cross-section oriented along the *a*-axis are created without guest water or ethanol molecules (Figure 1c). The node−node distances are 4.869(2), 7.682(3), and 7.682(3) Å, respectively. The neutral 3-D nanoporous network can also be considered as being constructed from distorted two-dimensional (2-D) square-grid (4,4) layers (Figure 1d), which are cross-linked by zigzag chains. These MOFs with microporosity might be good candidates for storage of small molecules like hydrogen, and further investigation will be performed. As far as we known, the numerous

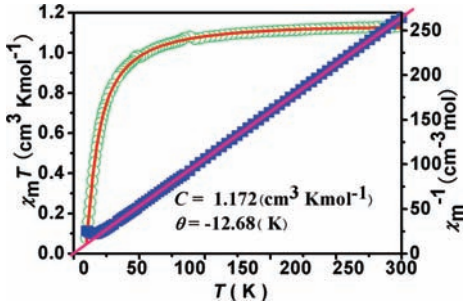

Figure 2. Temperature dependence of $\chi_m T$ vs T. Solid line represents the best theoretical fit for complex **1**.

MOFs of α-Po topology are 2-fold or 3-fold interpenetrated frameworks.[1,32−41] Complexes **1**−**3** are the scarce examples of non-interpenetrated structures of the topology. The topologies of these complexes are similar to $Zn_2(trz)_2(ox)$ which are constructed from comparable (4,4) layers that are further connected to 3-D networks by bridging ligands.[42]

Magnetic Properties of the Complexes 1 and 2. The magnetic susceptibility of complex **1** has been measured in the temperature range of 2−300 K at an applied field of 5000 Oe, with the plots of χ_m^{-1} vs T and $\chi_m T$ vs T shown in Figure 2. At 300 K, $\chi_m T$ is 1.14 cm^3 K mol^{-1} (3.07 μ_B) in agreement with the reported value for complex of Ni(II) ions in a distorted octahedral coordination.[43] As the temperature decreases, the value remains essentially constant until 100 K. However, the value decreases rapidly as the temperature decreases below 100 K, and then reaches a value of 0.08 cm^3 K mol^{-1} at 2 K. The decrease in $\chi_m T$ vs T values with decreasing temperature is an indication of antiferromagnetic coupling between the metal ions in complex **1**. The $1/\chi_m$ versus T plot above 16.8 K obeys the Curie−Weiss law $\chi_m = C/(T - \theta)$ with a Weiss constant $\theta = -12.7$ K and a Curie constant $C = 1.17$ cm^3 K mol^{-1}. The negative θ confirms intramolecular antiferromagnetic coupling.

The smallest separation (4.87 Å) of M−M in the intrachain is much shorter than that (7.68 Å) between chains, which is analogous with $\{(H_3O)[Ni(H_2L)]_2[Fe(CN)_6]_2 \cdot [Fe(CN)_6] \cdot 6H_2O\}_n$,[44] as a result, the possible magnetic superexchange pathway is mainly inside the 1-D chain. The magnetic susceptibility of complex **1** may be fitted by using Fisher equations[45−47] based on the spin Hamiltonian $H = -J\sum_i S_i S_{i+1}$, which has been successfully used for some Ni complexes such as

(32) Soma, T.; Yuge, H.; Iwamoto, T. *Angew. Chem., Int. Ed.* **1994**, *33*, 1665.
(33) Duncan, P. C. M.; Goodgame, D. M. L.; Menzer, S.; Williams, D. J. *Chem. Commun.* **1996**, 2127.
(34) Siebel, E.; Fischer, R. D. *Chem.—Eur. J.* **1997**, *3*, 1987.
(35) Plater, M. J.; Foreman, M. R. S.; Skakle, J. M. S. *Cryst. Eng.* **2001**, *4*, 293.
(36) Abrahams, B. F.; Hoskins, B. F.; Robson, R.; Slizys, D. A. *CrystEngComm* **2002**, *4*, 478.
(37) Jensen, P.; Batten, S. R.; Moubaraki, B.; Murray, K. S. *Dalton Trans.* **2002**, 3712.
(38) Niel, V.; Munoz, M. C.; Gaspar, A. B.; Galet, A.; Levchenko, G.; Real, J. A. *Chem.—Eur. J.* **2002**, *8*, 2446.
(39) Lu, W. J.; Zhang, L. P.; Song, H. B.; Wang, Q. M.; Mak, T. C. W. *New J. Chem.* **2002**, *26*, 775.
(40) Yang, S. Y.; Long, L. S.; Jiang, Y. B.; Huang, R. B.; Zheng, L. S. *Chem. Mater.* **2002**, *14*, 3229.
(41) Abrahams, B. F.; Batten, S. R.; Hoskins, B. F.; Robson, R. *Inorg. Chem.* **2003**, *42*, 2654.
(42) Zhai, Q. G.; Lu, C. Z.; Wu, X. Y.; Batten, S. R. *Cryst. Growth Des.* **2007**, *7*, 2332.
(43) Roth, A.; Buchhoz, A.; Rudolph, M.; Schuetze, E.; Kothe, E.; Plass, W. *Chem.—Eur. J.* **2008**, *14*, 1571.
(44) Kou, H. Z.; Zhou, B. C.; Liao, D. Z.; Wang, R. J.; Li, Y. D. *Inorg. Chem.* **2002**, *41*, 6887.
(45) Fisher, M. E. *Am. J. Phys.* **1964**, *32*, 343.
(46) Kahn, O. *Molecular Magnetism*; VCH: New York, 1993.
(47) Carlin, R. L. *Magnetochemistry*; Springer, Berlin, Heidelberg, 1986.

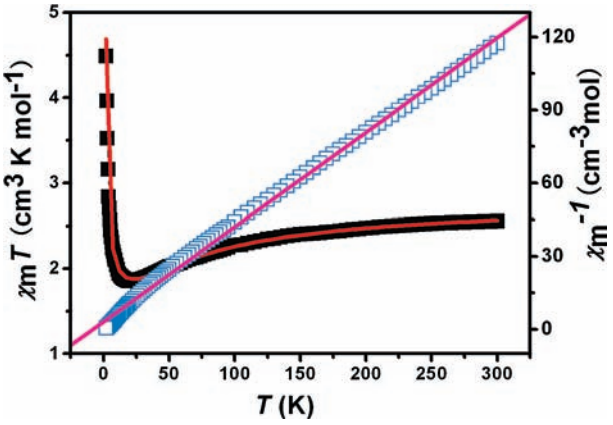

Figure 3. Plot of $\chi_m T$ and χ_m^{-1} vs T for complex **2**. Solid line represents the best theoretical fit for complex **2**.

$Ni(baepn)(CN)]_n(ClO_4)_n$,[48] $\{(H_3O)[Ni(H_2L)]_2[Fe(CN)_6]_2 \cdot [Fe(CN)_6] \cdot 6H_2O\}_n$,[44] $\{[Ni_2L_2(H_2O)_4] \cdot 3H_2O\}_n$,[49] and so on. In the case of complex **1**, considering the influence of the collaboration of zero field splitting and interchain magnetic superexchange, the mean field correction was taken into account for the classical $S = 1$ spin chain system:

$$u = \coth[JS(S+1)/(k_B T)] - [k_B T/(JS(S+1))] \quad (1)$$

$$\chi_{chain} = [Ng^2\beta^2 S(S+1)/(3kT)] \cdot [(1+u)/(1-u)] \quad (2)$$

$$\chi_m = \frac{\chi_{chain}}{1 - \chi_{chain}(2zJ'/Ng^2\beta^2)} \quad (3)$$

In this model, χ_m is the exchange coupled magnetic susceptibility actually measured, χ_{chain} is the magnetic susceptibility in the absence of the exchange field, and zJ' is the mean field parameter. The rest of the parameters have their usual meanings. This model turned out to be satisfactory in this case, based on $g = 2.14$, obtained from EPR results (Supporting Information, Figure S2), we got the best-fit parameters: $J = -6.09$ (standard deviations: 4.46×10^{-4}) cm^{-1}, $zJ' = 2.01$ (standard deviations: 8.70×10^{-2}) cm^{-1}, and the agreement factor $R = 8.02 \times 10^{-6}$, where $R = [(\chi_m)_{obsd} - (\chi_m)_{calcd}]^2/[(\chi_m)_{obsd}]^2$. The negative J values are consistent with the occurrence of an antiferromagnetic coupling between the Ni(II) ions.

The measurement of the thermal variation of the magnetic susceptibility was performed on a crystalline sample of complex **2** in the range of 2−300 K in an applied field of 1000 Oe. The plots of $\chi_m T$ and $1/\chi_m$ versus T are shown in Figure 3. The $\chi_m T$ value at room temperature (2.57 cm^3 K mol^{-1}) is significantly greater than the spin-only value for a high-spin Co(II) center (1.88 cm^3 K mol^{-1} for $S = 3/2$ and $g = 2.0$), while it agrees with the values observed for high-spin Co(II) complexes in an octahedral surrounding with a significant first-order orbital contribution to the magnetic moment.[50−52] The value of $\chi_m T$ decreases gradually to a minimum of 1.88 cm^3 K mol^{-1} at 22 K. Below this temperature, the $\chi_m T$ value increases abruptly and reaches a maximum of 4.69 cm^3 K mol^{-1} at 2 K, indicating the ferromagnetic coupling in complex **2**. The temperature dependence of magnetic susceptibilities above 2 K follows the Curie−Weiss law $\chi_m = C/(T - \theta)$ with a Weiss constant $\theta = -8.18$ K and a Curie constant $C = 2.60$ cm^3 mol^{-1} K. The Curie constant is much larger than the expected spin-only value, indicating that the orbital contribution of Co^{2+} ions exists in complex **2**. Thereby the negative value of θ is incapable of indicating the antiferromagnetic coupling between Co^{2+} ions because of the strong spin−orbital coupling through the $^4T_{1g}$ state of the octahedral Co^{2+} centers.

A detailed quantitative analysis of the susceptibility data for Co^{2+} complexes is often complicated by the fact that the orbital moment, spin−orbit coupling, distortions from regular stereochemistry, electron delocalization, and crystal field mixing of excited states into the ground state affect the magnetic properties (in addition to a possible magnetic interaction).[46] In present case, several models turned out to be unsatisfactory, such as the Heisenberg model and the above-mentioned Fisher 1-D chain model for a one-dimensional chain of $S_{Co} = 3/2$, because it does not take into account the effects of the spin−orbit coupling for octahedral Co(II) complexes ($^4T_{1g}$ ground state). Previous magnetic reports[46,47] showed that some 1-D systems of cobalt(II) are associated with anisotropic Ising systems with an effective spin $S = 1/2$, and they can be fitted at low temperature range ($T < 30$ K) where only the ground Kramer's doublet is thermally populated.[53,54] This model turned out to be unsatisfactory as the exchange interaction is too weak to show up clearly against the spin−orbit coupling.[55,56]

Recently, Rueff et al.[57,58] have proposed a phenomenological approach for some low-dimensional Co^{2+} systems that allows one to have an estimate of the strength of the antiferromagnetic exchange interactions by means of the equation: $\chi_m T = A \exp(-E_1/(kT)) + B \exp(-E_2/(kT))$. Herein, $A + B$ equals the Curie constant, and E_1 and E_2 represent the "activation energies" corresponding to spin−orbit coupling and the antiferromagnetic exchange interaction. This equation adequately describes the spin−orbit coupling (high-temperature region) and the exponential low-temperature divergence of the susceptibility.[55,56] It turns out to be useful in our present work. The results obtained from the Rueff procedure are excellently consistent with the experimental data. The best fit parameter is $R = 1.17 \times 10^{-3}$, where

(48) Koo, J.; Kim, D.; Kim, Y. S.; Do, Y. *Inorg. Chem.* **2003**, *42*, 2983.
(49) Yao, Y. L.; Che, Y. X.; Zheng, J. M. *Cryst. Growth Des.* **2008**, *8*, 2299.
(50) Lu, J. Y.; Lawandy, M. A.; Li, J.; Yuen, T.; Lin, C. L. *Inorg. Chem.* **1999**, *38*, 2695.
(51) Zheng, L. M.; Fang, X.; Lii, K. H.; Song, H. H.; Xin, X. Q.; Fun, H. K.; Chinnakali, K.; Razak, I. A. *Dalton Trans.* **1999**, 2311.
(52) Garcia-Couceiro, U.; Castillo, O.; Luque, A.; Beobide, G.; Roman, P. *Inorg. Chim. Acta* **2004**, *357*, 339.
(53) Fisher, M. E. *J. Math. Phys.* **1963**, *4*, 124.
(54) Angelow, S.; Drillon, M.; Zhecheva, E.; Stoyanova, R.; Belaiche, M.; Derory, A.; Herr, A. *Inorg. Chem.* **1992**, *31*, 1514.
(55) Rueff, J. M.; Masciocchi, N.; Rabu, P.; Sironi, A.; Skoulios, A. *Eur. J. Inorg. Chem.* **2001**, 2843.
(56) Rueff, J. M.; Masciocchi, N.; Rabu, P.; Sironi, A.; Skoulios, A. *Chem.—Eur. J.* **2002**, *8*, 1813.
(57) Cabrero, J.; Ben Amor, N.; de Graaf, C.; Illas, F.; Caballol, R. *J. Phys. Chem. A* **2000**, *104*, 9983.
(58) Cano, J.; Alemany, P.; Alvarez, S.; Verdaguer, M.; Ruiz, E. *Chem.—Eur. J.* **1998**, *4*, 476.

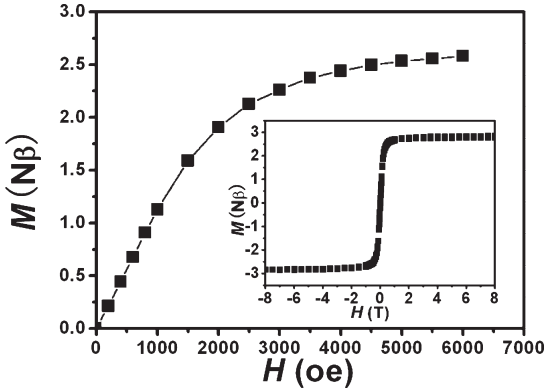

Figure 4. Field dependence of magnetization for complex **2** at 1.8 K (inset: magnetic hysteresis loop at 1.82 K for complex **2**).

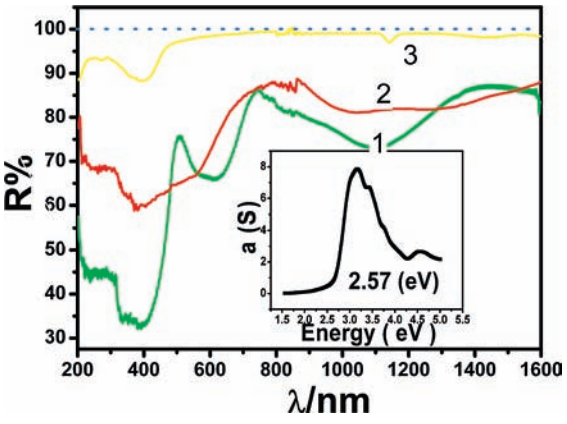

Figure 5. Optical absorption spectra of complex **1**−**3** (inset: diffuse reflectance spectrum of complex **3**).

$R = [(\chi_m)_{obsd} - (\chi_m)_{calcd}]^2/[(\chi_m)_{obsd}]^2)$. The $A + B$ value is 2.79 (standard deviations: 1.4×10^{-2}) cm^3 mol^{-1} K, which agrees well with those given in the literature for the Curie constant ($C = 2.8-3.5$ cm^3 K mol^{-1}). E_1/k, the effect of spin−orbit coupling and site distortion, is +69.5 (standard deviations: 1.53) K, which is consistent with the values reported by Rueff et al. for several 1-D and 2-D Co^{2+} complexes.[55,56] The best-fit $-E_2/k$ is 2.06 (standard deviations: 1.39×10^{-2}) K, corresponding to interactions $J = 4.12$ K within the Ising chain approximation ($XT \propto \exp(+J/2kT)$.[55,56] These results illuminate that the ferromagnetic exchange between Co^{2+} ions is transmitted by hydrazine groups.

The M versus H plot of complex **2** at 2 K is shown in Figure 4. In the low-field region, the magnetizations increase slowly with increasing field; subsequently, they increase abruptly and finally reach saturation plateaus with a fast saturation of the magnetization (2.85 Nβ at 8 T), which is consistent of the saturation value concurring with the theoretical range (2−3 Nβ) expected for Co (II) complexes. No detectable magnetic hysteresis manifests the absence of magnetic ordering.

Spectroscopic Properties. UV−vis diffuse reflective spectra, emission spectra, and the luminescence under ultraviolet light illumination at room temperature of complex **3** are shown in Figure 5 and Figure 6, respectively. The absorption of the complex **3** has a weak absorption peaked at ~273 nm and an intense absorption band centered at ~393 nm, which can be ascribed to

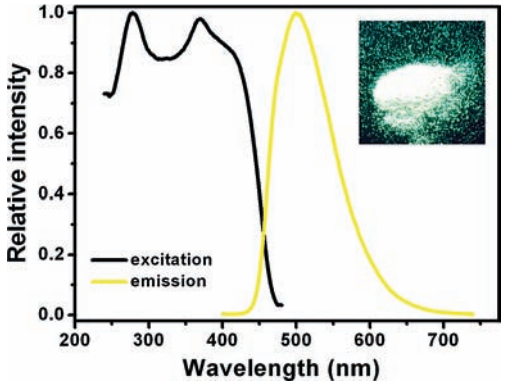

Figure 6. Solid-state electronic emission spectra of complex **3** at room temperature (inset: luminescence of complex **3** under ultraviolet light illumination at room temperature).

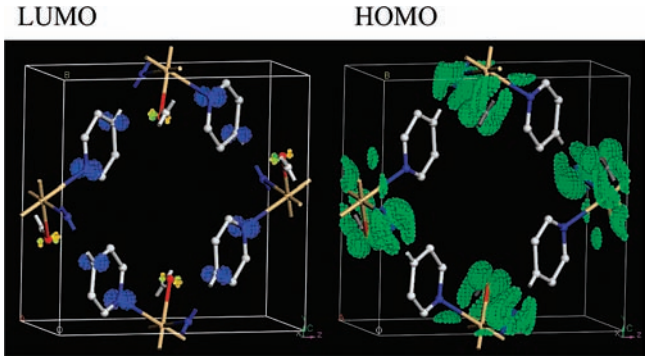

Figure 7. Electron-density distribution of the LUMO and HOMO calculated for complex **3**.

intraligand $\pi-\pi^*$ transition. The complex **3** displays a very strong fluorescent emission band at 501 nm in the solid state at room temperature. The lifetime of the emission is 2.5 ns. A better insight of the nature of the fluorescence properties can be achieved by theoretic calculation. The density functional theory (DFT) calculations[25−28] were performed by using the CASTEP code.[29] The results further indicate that the emission of complex **3** can be assigned to intraligand $\pi-\pi^*$ transition. As shown in Figure 7, both the highest occupied molecular orbital (HOMO) and the lowest unoccupied molecular orbital (LUMO) have ligand character. A π orbital of the pyridyl group makes mainly contribution to the LUMO, while the HOMO consists of the delocalized π-orbital conjugated system of hydrazine -(CO)NN(CO)− moiety. A band structure of complex **3** calculated by using DFPT within the local density approximation (LDA) gives a band gap of 2.17 eV (Figure 8), which is comparable to the experimental optical gap of 2.57 eV (Figure 5). On the basis of the time-dependent perturbation theory of spectroscopy, the probability of radiative transition is apparently increased in the metal coordination polymer.[59] The intense luminescence for complex **3** may be attributed to the strong interaction existing between the ligand and the metal, especially, a new formed π-electron conjugated system of −(CO)NN(CO)− moiety with more extended delocalization environment by the metal

(59) Lakowicz, J. R. *Principles of Fluorescence Spectroscopy*; Plenum Press: New York, 1983.

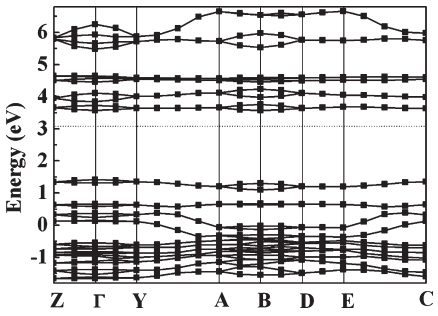

Figure 8. Band structure of complex **3** calculated using DFPT within the local density approximation (LDA).

coordination. Owing to the optimization of the delocalization environment and a narrow $\pi-\pi^*$ energy gap induced by the newly formed π-electron system, the transition of the HOMO−LUMO becomes relatively easy. On the other hand, the strong luminescence for complex **3** may also be attributed to two chelating L ligands in the equatorial plane of an octahedral metal center. The chelating coordination effectively increases the rigidity of the ligands and also reduces the loss of energy by non-radiative decay. Although complexes **1**−**3** are isostructural, complexes **1**−**2** have no luminescence, because of their different metal centers. Co(II) and Ni(II) complexes are characterized by d^7 and d^8 electronic configurations, respectively, and show relatively intense metalcentered (MC) absorption bands in the vis-NIR spectral window (Figure 5), which deactivate via ultrafast non-radiative pathways.[60] The above experimental facts suggest that complex **3** is a good potential candidate for hybrid inorganic−organic photoactive materials while complexes **1**−**2** are not of any interest for luminescence-related applications.

Thermogravimetric Analysis (TGA) and XRPD. The thermal stabilities of complexes **1**−**3** were investigated on crystalline samples under nitrogen atmosphere from 30 to 1200 °C. The TG curves of the three complexes are similar, as shown in Supporting Information, Figure S3. The thermogravimetric analysis (TGA) study shows that the three complexes decompose at a decomposition point *T* onset of 456, 423, and 523 °C, respectively, indicating that the present complexes are stable enough for further application. The XRPD patterns of complexes **1**−**3** are shown in Supporting Information, Figures S4−S6. The agreement of the experimental and simulated XRPD patterns demonstrates that the porous network of complex **1** is retained after being dried at 350 °C under vacuum (Supporting Information, Figure S4). The detailed decomposition mechanisms of the three complexes are too complex to explain at the current conditions, and further investigation was needed.

(60) Barbieri, A.; Accorsi, G.; Armaroli, N. *Chem. Commun.* **2008**, 2185.

Conclusion

The use of L to react with transition metal salts, through the metal-assisted hydrolysis of L, affords a series of interesting self-assembled polymeric architectures. The overall topology of the 3-D MOFs can be described as a noninterpenetrated α-Po net, which is built from parallel (4,4) nets cross-linked by zigzag chains. As a consequence, 1-D rhombus channels without guest water or ethanol molecules are formed. Although the three complexes are isomorphic, some of their physical properties are quite different. Complex **1** shows intra- and intramolecular antiferromagnetic coupling while complex **2** shows overall ferromagnetic coupling between the metal centers. Complex **3** exhibits strong fluorescence emission bands in the solid state at room temperature. The polymers may exhibit novel properties in luminescence and magnetism through using different transition metals. In addition, these complexes also demonstrate that the use of L to react with transition metals through a ring-opening reaction is an effective strategy to construct MOFs with intriguing architectures.

Acknowledgment. This work was supported by the 973 key program of the MOST (2006CB932904, 2007CB815304), the National Natural Science Foundation of China (20425313, 20521101, and 50772113), the Chinese Academy of Sciences (KJCX2-YW-M05), the Natural Science Foundation of Fujian Province (2006F3135, 2006F3141), and the Fund of Fujian Key Laboratory of Nanomaterials (2006L2005).

Supporting Information Available: Additional magnetic data plots for complex **2**, X-ray crystallographic files in CIF format, IR and EPR spectra, TG curves, experimental and simulated X-ray powder diffraction patterns for complexes **1**−**3** are presented. This material is available free of charge via the Internet at http://pubs.acs.org.